J|A|C|S
ARTICLES
Published on Web 05/12/2006

Electrochemistry at Single-Walled Carbon Nanotubes: The Role of Band Structure and Quantum Capacitance

Iddo Heller, Jing Kong,† Keith A. Williams,‡ Cees Dekker, and Serge G. Lemay*

Contribution from the Kavli Institute of Nanoscience, Delft University of Technology, Lorentzweg 1, 2628 CJ Delft, The Netherlands

Received February 20, 2006; E-mail: lemay@mb.tn.tudelft.nl

Abstract: We present a theoretical description of the kinetics of electrochemical charge transfer at single-walled carbon nanotube (SWNT) electrodes, explicitly taking into account the SWNT electronic band structure. SWNTs have a distinct and low density of electronic states (DOS), as expressed by a small value of the quantum capacitance. We show that this greatly affects the alignment and occupation of electronic states in voltammetric experiments and thus the electrode kinetics. We model electrochemistry at metallic and semiconducting SWNTs as well as at graphene by applying the Gerischer−Marcus model of electron transfer kinetics. We predict that the semiconducting or metallic SWNT band structure and its distinct van Hove singularities can be resolved in voltammetry, in a manner analogous to scanning tunneling spectroscopy. Consequently, SWNTs of different atomic structure yield different rate constants due to structure-dependent variations in the DOS. Interestingly, the rate of charge transfer does not necessarily vanish in the band gap of a semiconducting SWNT, due to significant contributions from states which are a few k_BT away from the Fermi level. The combination of a nanometer critical dimension and the distinct band structure makes SWNTs a model system for studying the effect of the electronic structure of the electrode on electrochemical charge transfer.

Introduction

Carbon is widely used as electrode material for electrochemistry. The combination of a wide useful potential window, electronic properties similar to metals, and its versatile organic chemistry make sp^2 carbon a special electrode material.[1] Recently, there has been a large interest in using single-walled carbon nanotubes (SWNTs) as electrodes for electrochemistry.[2−4] This interest mostly originates from the prospect of using individual SWNTs as carbon nanoelectrodes or ensembles of SWNTs as large surface-area carbon electrodes. The molecules' interesting, unconventional electronic properties, however, are often neglected. Depending on their chirality, SWNTs behave either as a metal or a semiconductor. They possess a distinct and nontrivial density of electronic states (DOS) displaying van Hove singularities typical for one-dimensional conductors,[5−7] as has been observed in STM spectroscopy.[8,9] It has been demonstrated that semiconducting SWNTs can act as channels in nanoscale transistors, allowing their conductance to be tuned by electrostatic interaction with a solid-state gate[10] or an electrolyte gate.[11] A potential applied between an SWNT and the electrolyte it is immersed in can very effectively change the chemical potential of the SWNT. Since this interfacial potential difference drives electrochemical reactions in voltammetric experiments, electrolyte gating and electrochemical charge transfer are inevitably coupled.

In previous work, we demonstrated that individual SWNTs can be used as nanoelectrodes for electrochemistry, yielding enhanced mass transport and high current densities equivalent to sub-10 nm hemispherical electrodes.[2] Due to their nanometer critical dimension, electrode kinetics are accessible even for fast electrode reactions such as the oxidation of ferrocenes. Since the kinetics of electrochemical charge transfer are affected by the occupation and alignment of electronic states in solution and on the electrode,[12,13] it is important to understand in detail the effect of both electrolyte gating and a distinct electronic structure on electrochemistry at SWNTs.

In this paper, we introduce the relevant features of the electronic structure of SWNTs in the context of electrolyte

† Present address: Department of Electrical Engineering and Computer Science, Massachusetts Institute of Technology, 77 Massachusetts Avenue, Cambridge, MA 02139-4307.

‡ Present address: Department of Physics, University of Virginia, 382 McCormick Road, Charlottesville, VA 22904-4714.

(1) McCreery, R. L. *Electrochemical properties of carbon surfaces*. ed.; Dekker: New York, 1999; p 631.
(2) Heller, I.; Kong, J.; Heering, H. A.; Williams, K. A.; Lemay, S. G.; Dekker: C. *Nano Lett.* **2005**, *5* (1), 137−142.
(3) Gooding, J. J. *Electrochim. Acta* **2005**, *50* (15), 3049−3060.
(4) Katz, E.; Willner, I. *ChemPhysChem* **2004**, *5*, 1048.
(5) Dekker, C. *Physics Today* **1999**, *52* (5), 22−28.
(6) Saito, R.; Fujita, M.; Dresselhaus, G.; Dresselhaus, M. S. *Appl. Phys. Lett.* **1992**, *60* (18), 2204−2206.
(7) Dresselhaus, M. S.; Dresselhaus, G.; Saito, R. *Solid State Commun.* **1992**, *84*, 201.
(8) Wildoer, J. W. G.; Venema, L. C.; Rinzler, A. G.; Smalley, R. E.; Dekker, C. *Nature* **1998**, *391* (6662), 59−62.
(9) Odom, T. W.; Huang, J. L.; Kim, P.; Lieber, C. M. *Nature* **1998**, *391* (6662), 62−64.
(10) Tans, S. J.; Verschueren, A. R. M.; Dekker, C. *Nature* **1998**, *393* (6680), 49−52.
(11) Rosenblatt, S.; Yaish, Y.; Park, J.; Gore, J.; Sazonova, V.; McEuen, P. L. *Nano Lett.* **2002**, *2* (8), 869−872.
(12) Adams, D. M. et al. *J. Phys. Chem. B* **2003**, *107*, 6668.
(13) Bard, A. J.; Faulkner, L. R. *Electrochemical Methods, Fundamentals and Applications*, 2nd ed.; John Wiley & Sons: New York, 2001.

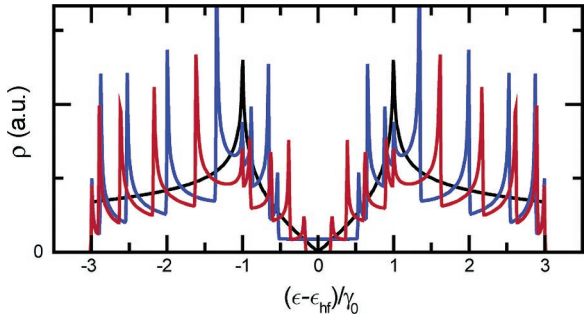

Figure 1. Nearest-neighbor tight-binding calculation of the density of electronic states (DOS) as a function of energy for a graphene sheet (black), a metallic (9,0) SWNT (blue), and a semiconducting (10,0) SWNT (red). $\gamma_0 = 2.7$ eV is the nearest-neighbor interaction energy.

gating. We combine electrochemical gating and electrochemical charge transfer by applying the Gerischer−Marcus model of heterogeneous electron transfer kinetics to SWNTs and show that the interfacial capacitances have a large impact on the behavior of electron transfer at SWNT electrodes. The potential-dependent rate of electron transfer reveals a rich spectrum, caused by the distinct SWNT band structure, allowing for a form of electrochemical spectroscopy to be performed. Due to atomic-structure-dependent variations of the features in the DOS, we predict relatively large differences between electron transfer rates at different SWNTs. We relate our calculations to classic Butler−Volmer kinetics in an experimentally relevant regime and observe a clear diameter-dependent trend in the apparent standard rate constant.

SWNT Electronic Density of States (DOS)

Graphene consists of a two-dimensional hexagonal lattice of sp^2 carbon, through which electronic conduction can occur via the π-conjugated electron system.[14] Graphene is sometimes classified as a zero-gap semiconductor, since the DOS per unit area, $\rho_{graph}(\epsilon)$, vanishes at the Fermi level. (For clarity we will use ϵ for energies, units eV, and V for voltages, units V.) The band structure of an SWNT can be described by considering the nanotube as a graphene sheet wrapped into a cylinder. The atomic structure of an SWNT is conventionally described by two indices (n,m) that fully define the radius and chirality.[5] The (n,m) indices also determine the electronic structure of the SWNT.[6] If $|n - m| = 3q$, where q is an integer, the SWNT is metallic, whereas for $|n - m| \neq 3q$ it is semiconducting and a band gap occurs in the DOS. The size of the band gap is inversely proportional to the diameter, yielding band gaps in the range 0.3 to 0.8 eV for SWNTs with diameters of 3 to 1 nm. Figure 1 shows nearest-neighbor tight-binding calculations of the π-electron DOS of a graphene sheet[14] and of a metallic and semiconducting SWNT.[6,7] The SWNT DOS roughly follows the graphene DOS but exhibits distinct singularities that are typical of one-dimensional electronic bands. These so-called van Hove singularities at energies ϵ_{vH} consist of a singular increase in the DOS followed by a $(\epsilon - \epsilon_{vH})^{-1/2}$ decrease. Because the van Hove singularities originate from the size-dependent quantization of electronic wave functions around the circumference of the SWNT, a smaller diameter of the SWNT leads to a larger energy spacing between subsequent van Hove singularities, analogous to energy level spacings in quantum dots. The

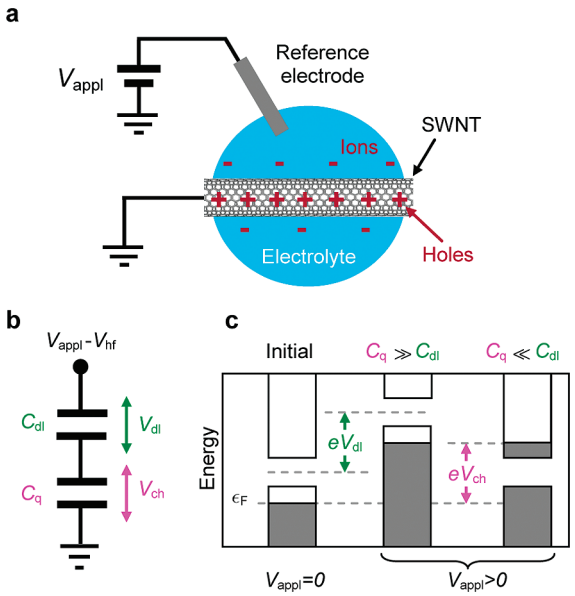

Figure 2. (a) Schematic representation of a measurement layout showing an SWNT submerged in an electrolyte. A potential V_{appl} is applied between the SWNT and a reference electrode in solution, inducing an electrical double layer at the SWNT−electrolyte interface. (b) The interfacial capacitance between SWNT and electrolyte can be represented as the electrostatic double-layer capacitance C_{dl} in series with the chemical quantum capacitance C_q. Although they are represented as linear circuit elements here, both are in fact nonlinear: $C_q = C_q(V_{ch})$ and $C_{dl} = C_{dl}(V_{dl})$. (c) Energy diagram showing the influence of the quantum capacitance on the alignment and occupation of electronic states in the SWNT. The reference energy in this diagram is set by the reference electrode. In the initial situation, the Fermi level is positioned in the valence band of the SWNT. In the classical case $C_q \gg C_{dl}$, application of a positive voltage $V_{appl} > 0$ will shift the band structure by eV_{dl} with respect to its initial position, while the position of the Fermi level with respect to the band edges remains unchanged. In the extreme opposite case, $C_q \ll C_{dl}$, the position of the band gap remains unchanged with respect to the reference energy, while the Fermi level shifts by eV_{ch} with respect to the bands.

typical positions of van Hove singularities are different for metallic and semiconducting SWNTs. At this level of approximation the DOS of SWNTs and graphene are symmetrical around the half-filling energy, ϵ_{hf}, defined as the energy at which all bonding orbitals are filled and all antibonding orbitals are empty, yielding exactly one occupied π-orbital per carbon atom.

Quantum Capacitance

SWNTs can be employed in a field-effect-transistor layout with an electrolyte in contact with the SWNT acting as a gate,[11] as illustrated in Figure 2a. Note that, to simplify the notation when relating energy changes to potential changes, we use the convention that potentials are applied to the reference electrode with respect to the working electrode. A potential V_{appl} applied between the SWNT and the electrolyte through a reference electrode in solution can cause a net charge to build up in the SWNT, which is screened by charge in the electrical double-layer in solution. The electrostatic capacitance of this interface is given by the capacitance of the electrical double-layer C_{dl}, which we approximate as $C_{dl} = \epsilon A/x_{OHP}$, with ϵ, the dielectric constant of water, A, the area of the exposed SWNT-surface, and x_{OHP}, the distance to the outer Helmholtz plane which is about 0.5 nm.[13,15] Typically C_{dl} is of the order of 10fF per μm length of SWNT. To account for the choice of reference

(14) Wallace, P. R. *Physical Review* **1947**, *71* (9), 622−634.

(15) In principle $C_{dl} = C_{dl}(V_{appl})$, but we ignore this complication for simplicity.

electrode and introduce a slight p-doping of the SWNT, we set V_{hf}, the potential at which $\epsilon_F = \epsilon_{hf}$ to 0.2 V with respect to a Ag/AgCl reference potential, in agreement with experimental data obtained from electrolyte gating.[11] In the simplest approach, ignoring effects of the finite DOS of the electrode, the potential drop over the double layer is $V_{dl} = V_{appl} - V_{hf}$.

SWNTs however have a rather low density of electronic states per unit energy around the Fermi level ϵ_F. This causes the average energy spacing between adjacent states to be much larger than that in common metals. While charging an SWNT upon applying a potential over the SWNT−electrolyte interface, one has to raise or lower the Fermi level by this large average energy spacing for each subsequent state that is filled or depleted. A significant part of the interfacial potential thus takes the form of a change of the chemical potential, V_{ch}, of the SWNT instead of an electrostatic potential drop over the double layer, such that $V_{appl} - V_{hf} = V_{ch} + V_{dl}$. This effect is analogous to electrochemistry at semiconductor electrodes, where band bending at the surface of the semiconductor causes part of an applied potential to appear as a chemical potential drop that significantly affects electrochemical reactions at the semiconductor surface. Because every atom in an SWNT is part of the surface and in contact with solution, however, the occupancy of electronic states is affected over the entire SWNT.

The contribution from a chemical potential drop over the SWNT−electrolyte interface can be modeled by introducing a second capacitance in series with the double layer capacitance, the quantum capacitance[11,16] C_q, which is related to the charge on the SWNT−double layer interface Q as $C_q(V_{ch}) = Q(V_{ch})/V_{ch}$. To evaluate $Q(V_{ch})$, we calculate the change in charge on the SWNT when its Fermi level shifts from $\epsilon_F = \epsilon_{hf}$ to $\epsilon_F = \epsilon_{hf} - eV_{ch}$; $Q(V_{ch}) = Ae \int_{-\infty}^{\infty} [f(\epsilon - \epsilon_{hf}) - f(\epsilon - \epsilon_{hf} - eV_{ch})]\rho(\epsilon - \epsilon_{hf})\, d\epsilon$, where $f(\epsilon)$ is the Fermi−Dirac distribution function, $f(\epsilon) = [1 + \exp(\epsilon/k_BT)]^{-1}$. C_q is of the order of 1fF per μm of SWNT. As illustrated in Figure 2b, $(V_{appl} - V_{hf})$ splits into an electrostatic part over the double layer capacitance, $V_{dl} = (V_{appl} - V_{hf})C_q/C_\Sigma$, and a chemical part over the quantum capacitance, $V_{ch} = (V_{appl} - V_{hf})C_{dl}/C_\Sigma$, where $C_\Sigma = C_q + C_{dl}$.

To illustrate the qualitative difference between a classical electrode, defined as an electrode for which the effect of a finite DOS is negligible and thus $C_q \gg C_{dl}$ (classical limit), and a quantum-capacitance-dominated electrode, where $C_q \ll C_{dl}$ (quantum limit), Figure 2c shows the energy diagrams for these two extremes. In the classical case, V_{appl} takes the form of an electrostatic potential drop over the double layer, shifting the full band structure in energy, while keeping the Fermi level at a fixed position with respect to the band edges. In the quantum limit, on the other hand, only the chemical potential of the electrode is altered. The band structure remains at the same energy, but the Fermi level is shifted. A rough calculation indicates that, for $V_{ch} < 1$V, $C_q < C_{dl}$ by at least an order of magnitude[11] and the quantum capacitance dominates. Consequently, the electrolyte acts as a highly efficient gate, able to induce considerable Fermi level shifts. Interestingly, since C_{dl} and C_q are in series, the total interfacial capacitance is lowered, causing a smaller amount of charge to accumulate at the interface, and lowering any interfacial electric fields. This description applies equally to metallic and semiconducting band structures; however, $C_q(V_{ch})$ is different for metallic and semiconducting SWNTs due to differences in band structure.

(16) Luryi, S. *Applied Physics Letters* **1988**, *52* (6), 501−503.

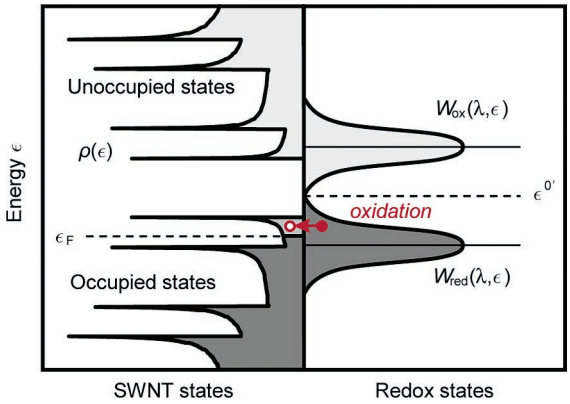

Figure 3. Energy diagram showing the energy overlap of the electronic states of electrode and solution in case $V_{ch} < 0$. Dark shaded areas indicate occupied electronic states, and light shaded areas indicate unoccupied electronic states. The left-hand side shows the electrode states represented by the density of electronic states of a semiconducting SWNT, $\rho(\epsilon)$. The right-hand side shows the redox states in solution represented by the Gaussian distributions of occupied reduced states, $W_{red}(\epsilon)$, and unoccupied oxidized states, $W_{ox}(\epsilon)$, centered around the standard energy of the redox couple $\epsilon^{0'}$. To illustrate an oxidation reaction, charge transfer is indicated by a red, horizontal arrow from an occupied redox state in solution to a vacant state on the electrode.

Gerischer−Marcus Model of Electrode Kinetics

To model electron transfer kinetics at electrodes with a nontrivial electronic structure, it is necessary to consider the distribution of electronic energy states in both electrode and solution. The Gerischer−Marcus model[13] takes into account that electron transfer may occur between molecular and electrode states provided that the process is elastic. In particular, charge transfer is not restricted to the Fermi level in this model. In the simplest, fully diabatic case, the energy distribution of oxidized and reduced states in solution, $W_{ox}(\epsilon)$ and $W_{red}(\epsilon)$, can be represented by Gaussian distributions with a standard deviation of $\sqrt{2\lambda k_B T}$ and means at $\epsilon^{0'} + \lambda$ and $\epsilon^{0'} - \lambda$, respectively, as illustrated in Figure 3, where λ is the reorganization energy and $\epsilon^{0'}$ is the energy corresponding to the formal potential of the redox couple $V^{0'}$. The local rate of oxidation at energy ϵ is proportional to the number of occupied states $W_{red}(\epsilon)$ in solution and the number of vacant states on the electrode $[1 - f(\epsilon - eV_{appl})]\rho(\epsilon - eV_{dl} - eV_{hf})$, where we use the convention that at $V_{appl} = 0$, $\epsilon_F = 0$ with respect to the reference energy. In this case, $\epsilon^{0'} = eV^{0'}$. By integration over all energies we obtain the reduction and oxidation rates, $k_{red} \propto \int_{-\infty}^{\infty} W_{ox}(\epsilon)\, f(\epsilon - eV_{appl})\, \rho(\epsilon - eV_{dl} - eV_{hf})\, d\epsilon$ and $k_{ox} \propto \int_{-\infty}^{\infty} W_{red}(\epsilon)[1 - f(\epsilon - eV_{appl})]\rho(\epsilon - eV_{dl} - eV_{hf})\, d\epsilon$. Since we are only interested in relative differences between different SWNTs, we have omitted a prefactor (normally assumed to be constant).[17]

Electrochemistry at SWNTs

In Figure 4 we show the results of a calculation of the rate of oxidation, k_{ox}, at a metallic SWNT, a semiconducting SWNT, and a graphene sheet, using the Gerischer−Marcus model of electrode kinetics. We use $V^{0'} = -0.25$ V for illustration, which

(17) Note that this prefactor is possibly potential-dependent; see ref 13. Nevertheless it is not likely to influence the qualitative effect of the electronic structure of the electrode on kinetics and is thus omitted for simplicity.

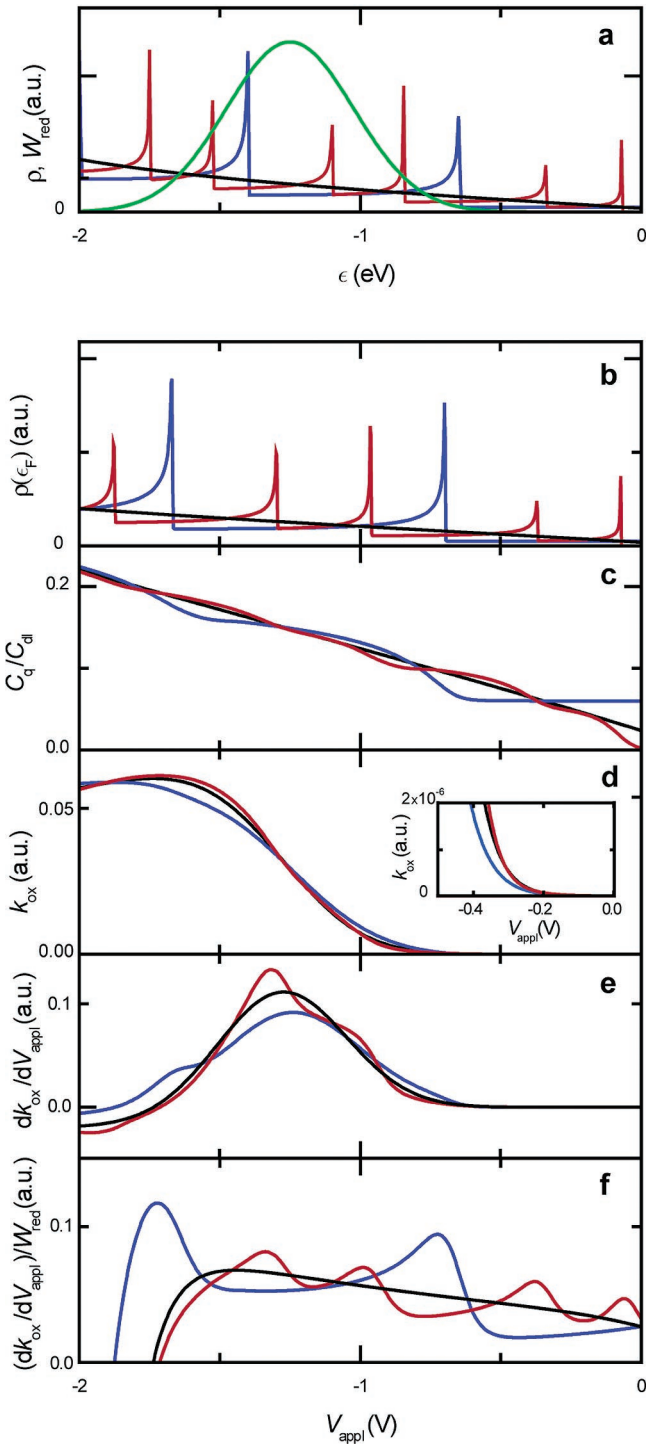

Figure 4. Calculations for electron transfer at a graphene sheet (black), a (10,10) metallic SWNT (blue), and a (10,11) semiconducting SWNT (red). For the calculations we used $V^{0'} = -0.25$ V, $\lambda = 1$ eV, and $V_{hf} = 0.2$ V. (a) Density of states as a function of energy. The green line shows the distribution of the reduced solution states. (b) Density of states at the Fermi level as a function of electrolyte gate potential. (c) Ratio of quantum and double-layer capacitances as a function of electrolyte gate potential. (d) Rate of oxidation, k_{ox}, as a function of applied potential. The inset shows k_{ox} near $V^{0'}$. (e) First derivative of the rate of oxidation as a function of electrolyte gate potential. (f) dk_{ox}/dV divided by W_{red} is plotted in order to retrieve the functional shape of the DOS as extractable from the rate of oxidation. Note the similarity of the peak positions to those in (b).

corresponds roughly to ferrocyanide. We use a relatively large reorganization energy $\lambda = 1$ eV for the redox molecules. Figure 4a shows the initial alignment of the distributions of electronic states of solution and electrodes at $V_{appl} = 0$, where the Fermi level is situated at $\epsilon = 0$. For SWNTs and graphene, the interfacial capacitance is largely determined by C_q, allowing substantial shifts of the Fermi level to occur as $|V_{appl}|$ increases. In Figure 4b the DOS at the Fermi level is plotted as a function of V_{appl}. Comparing Figure 4a and 4b shows that V_{appl} is not simply proportional to the energy due to the nonlinear quantum capacitance. Figure 4c shows the ratio of C_q/C_{dl}, which is of the order of 0.1. In Figure 4d we plot the calculated rate of oxidation k_{ox} as a function of V_{appl}. At $V_{appl} = 0$, k_{ox} is negligibly small because the occupied solution states (W_{red}) mostly overlap with occupied electrode states; see Figure 4a. As V_{appl} is made more negative, one can distinguish between two effects: For small V_{appl}, $C_q \ll C_{dl}$ (see Figure 4c), causing ϵ_F to shift with respect to the band structure, thereby vacating states to allow for the rate of oxidation to increase. Saturation of k_{ox} occurs as ϵ_F shifts into the Marcus-inverted region of W_{red}, $\epsilon_F < (\epsilon^{0'} - \lambda)$. A second effect can be observed for large V_{appl}, where the nonlinear $C_q(V_{ch})$ starts approaching C_{dl}. A significant part of V_{appl} then takes the form of an electrostatic potential drop over the double layer, shifting the DOS toward more negative energies, as shown in Figure 2c. Consequently, the peak of W_{red} is situated closer to ϵ_{hf}, where the DOS is lower, thus decreasing the total overlap integral and decreasing k_{ox}.

The differences among the three $k_{ox}-V_{appl}$ curves for a metallic SWNT, a semiconducting SWNT, and graphene are caused by the differences in the DOS of the three types of electrodes. This can be accentuated by plotting dk_{ox}/dV_{appl}, which reveals a rich spectrum, see Figure 4e. To obtain the structure of the DOS near the Fermi level from Figure 4e, in simplest approximation we divide dk_{ox}/dV_{appl} by W_{red}, as displayed in Figure 4f. Indeed, this plot reveals the sequence of van Hove singularities, which is broadened by both thermal energy and the change in electrostatic potential drop over the double layer. This approximation breaks down for $V_{appl} \lesssim -1.5$ V, since for those voltages the DOS has shifted considerably with respect to W_{red}, but the fingerprint of the distinct van Hove singularities in the rate of electrochemical charge transfer is clearly visible for smaller overpotentials. This indicates that voltammetry can in principle function as a form of single-molecule electrochemical spectroscopy at room temperature.

In Figure 4 we have used a relatively large reorganization energy of 1 eV. The reorganization energy and temperature define the position and width of the Gaussian distribution of the energies of the redox-states. DOS-effects are most pronounced in the potential region near the peak of the Gaussian since here the potential-dependent change in rate of reaction is largest. Consequently, a smaller reorganization energy would narrow the Gaussian distribution and thus reduce the potential range over which DOS effects can be resolved.

Quantum Capacitance and Electrode Kinetics

To further illustrate the significant influence that the quantum capacitance has on electrode kinetics at SWNTs, Figure 5 shows the calculation of the rate of oxidation for graphene and a semiconducting SWNT according to the Gerischer−Marcus model in the hypothetical extreme cases $C_q \gg C_{dl}$ (classical limit, dashed lines) and $C_q \ll C_{dl}$ (quantum limit, dash−dotted lines). In the classical case, a change of V_{appl} shifts all electrode states with respect to solution states by $e\Delta V_{dl} = e\Delta V_{appl}$, while

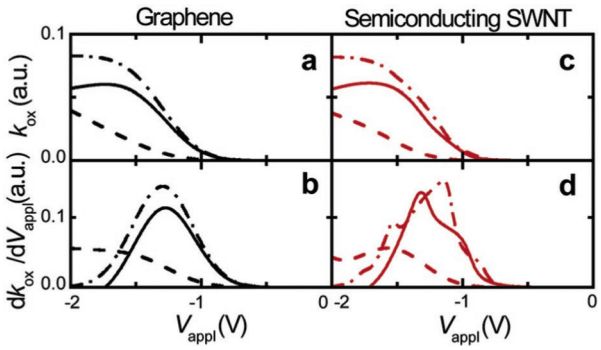

Figure 5. Calculations for electron transfer at a graphene sheet (a, b) and at a (10,11) semiconducting SWNT (c, d). Dashed lines indicate the classical limit $C_q \gg C_{dl}$, dash-dotted lines indicate the quantum limit $C_q \ll C_{dl}$, and solid lines indicate the realistic situation of Figure 4 where $C_{dl} \approx 10C_q(V)$. (a) and (c) display the calculated rate of oxidation as a function of electrolyte gate potential, while (b) and (d) display the first derivative of the rate of oxidation, k_{ox}, as a function of electrolyte gate potential. For all calculations we used $V^{0'} = -0.25$ V, $\lambda = 1$ eV, and $V_{hf} = 0.2$ V.

the chemical potential remains unchanged, $V_{ch} = 0$. This implies that k_{ox} is a convolution of $[1 - f(\epsilon - eV_{appl})]\rho(\epsilon - eV_{appl} - eV_{hf})$ and $W_{red}(\epsilon)$. Consequently, k_{ox} directly reflects the DOS of the SWNT, though broadened on a scale given by the width of $W_{red}(\epsilon)$, which is of the order of $\sqrt{2\lambda k_B T}$; see Figure 5a and c. In the quantum limit however, $C_q \ll C_{dl}$ and ΔV_{appl} only changes the occupancy of the electronic states, while the bands remain fixed to $W_{red}(\epsilon)$, resulting in the convolution of $W_{red}(\epsilon)\rho(\epsilon - eV_{hf})$ and $[1 - f(\epsilon - eV_{appl})]$. Thus k_{ox} roughly displays a sigmoidal shape (Figure 5a and c), saturating after ϵ_F has crossed into the Marcus inverted region. In dk_{ox}/dV however (Figure 5b and d), one obtains $W_{red}(\epsilon)\rho(\epsilon - eV_{appl})$, broadened on a scale of k_BT (~27 meV at room temperature), allowing for individual van Hove singularities to be observed. Although in both classical and quantum limits the rate constant depends on the positions of the van Hove singularities, a larger smearing occurs in the classical limit. The features due to the SWNT DOS in Figure 4e are visible with a broadening merely of the order of k_BT, only because $C_q(V_{ch}) < C_{dl}$ in the realistic case of Figure 4.

Nonzero Charge-Transfer Rate when $\rho(\epsilon_F) = 0$

Interestingly, even when a semiconducting SWNT is in the "off" state (the Fermi level resides in the band gap, and $\rho(\epsilon_F) = 0$), the interfacial transfer rate can still be nonzero. Because the Gerischer−Marcus model explicitly accounts for electron transfer that occurs at states away from the Fermi level, electrons from solution are allowed to tunnel into or out of the conduction or valence band. According to this model, the often expressed statement that electron transfer is inhibited due to the absence of states at the Fermi level for semiconducting SWNTs or graphite is overly simplified. More correctly, the rate of reaction is predicted to remain *constant* over the range of V_{appl} where $\rho(\epsilon_F) = 0$: When V_{appl} is varied, the total overlap integral of solution and electrode states remains unchanged since no new states occupy/vacate to allow charge transfer, nor does the alignment of solution and electrode states change. A finite electron-transfer rate can still be accommodated by tunneling into the states in conduction or valence bands. Since in the case of an SWNT the width of the band gap is of the same order of magnitude as the reorganization energy, the electrochemical current can be substantial. In Figure 6 we show the calculation

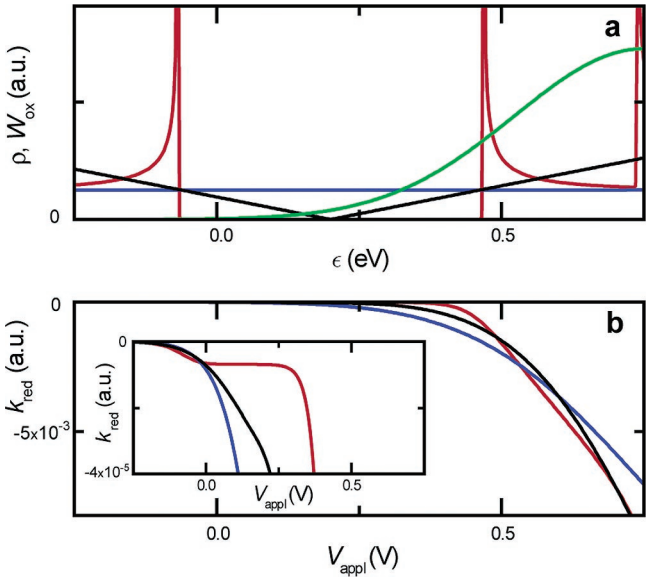

Figure 6. Calculations for a *reduction* reaction at a graphene sheet (black), a (10,10) metallic SWNT (blue), and a (10,11) semiconducting SWNT (red). (a) Density of states as a function of energy. The green line shows the distribution of the oxidized solution states. (b) Rate of reduction k_{red} as a function of applied potential. The inset shows the rate of reduction near V_{hf}. We used $V^{0'} = -0.25$ V, $\lambda = 1$ eV, and $V_{hf} = 0.2$ V.

of the rate of *reduction* k_{red}, instead of oxidation, under conditions identical to those for Figures 4 and 5. As illustrated in Figure 6a, the distribution of oxidized states, $W_{ox}(\epsilon)$, is positioned close to ϵ_{hf}. As a result, the DOS near ϵ_{hf} strongly affects the rate of reduction. Figure 6b shows that while a metallic SWNT yields an approximately exponential $k_{red}-V_{appl}$ curve, graphene displays a minor stalling of the increase in $|k_{red}|$ as ϵ_F sweeps through the minimum in the DOS. A semiconducting SWNT even reveals a plateau in the $k_{red}-V_{appl}$ curve as the Fermi level crosses the band gap. In general, large differences in curve shape between metallic and semiconducting SWNTs only occur in this special case where the Fermi level is positioned within the band gap of the semiconductor.

The calculations in Figure 6 show that a considerable rate of electron transfer remains for graphene even when $\epsilon_F = \epsilon_{hf}$. Although a number of studies indicate that basal plane graphite, which consists of stacked layers of graphene, yields a rate constant several orders of magnitude smaller than that of edge plane graphite or standard metal electrodes,[1,19] our modeling indicates that this cannot be explained by a mere lack of electronic states on the electrode to participate in charge transfer when $\epsilon_F = \epsilon_{hf}$, since states away from the Fermi level have significant contributions. This leads us to suggest that the observed behavior may be due to the electronic wave function overlap at the graphite surface, which affects the tunneling probability (i.e., part of the prefactor that is not explicitly calculated here).

Comparison to Butler−Volmer Kinetics

From our calculations, it is clear that the electronic structure of the electrode has a significant impact on heterogeneous electrode kinetics. More specifically, the positions of van Hove

(18) Day, T. M.; Wilson, N. R.; Macpherson, J. V. *J. Am. Chem. Soc.* **2004**, *126*, 16724.
(19) Davies, T. J.; Hyde, M. E.; Compton, R. G. *Angew. Chem., Int. Ed.* **2005**, *44*, 5121.

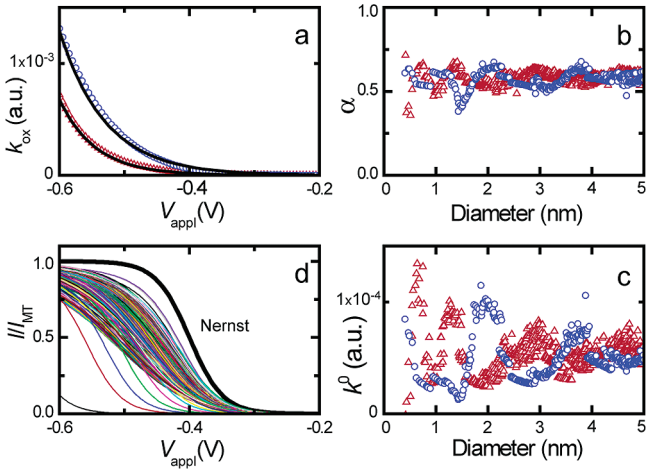

Figure 7. Intrinsic differences in electrode kinetics between SWNTs of different chirality and diameter at small overpotential are analyzed by comparing our calculations of k_{ox} to Butler−Volmer kinetics. (a) Fit of the Butler−Volmer equation of electrode kinetics to calculated $k_{ox}-V_{appl}$ curves of (10,10) metallic and (10,11) semiconducting SWNTs over a potential range of $-0.6\ V < V_{appl} < -0.2\ V$, using the transfer coefficient α and the standard rate constant k^0 as fitting parameters. Butler−Volmer fitting parameters α and k^0 are plotted as a function of SWNT diameter in (b) and (c), respectively. The fits were performed to the calculated $k_{ox}-V_{appl}$ curves for SWNTs of all possible chiralities over a diameter range between 0.4 nm and 5 nm. Each point represents one SWNT with unique chirality (n,m). (d) Voltammetric $I-V$ curves normalized by the diffusion-limited current I_{MT}, for all SWNTs of (b) and (c), calculated by combining the calculated rate of oxidation with the thermodynamic Nernst equation and mass transport limitation. The black line indicates the Nernstian limit. For all curves, we used $V^{0'} = -0.4$ V, and $V_{hf} = 0.2$ V. The few curves that display very low currents in the plotted potential range correspond to the smallest diameter semiconducting SWNTs that have a very wide band gap.

singularities and the band gap determine the $k - V$ characteristic. Since the position of van Hove singularities and the occurrence of a band gap in the DOS are entirely dependent on the chiral angle and diameter of the SWNT, properties that to date cannot be fully controlled in SWNT synthesis, intrinsic variations originating from differences in atomic structure are expected. We have previously shown experimentally that one can access electrode kinetics using SWNTs.[2] However, because of mass-transport limitations for the studied system, information on kinetics could only be obtained within a narrow potential range around $V^{0'}$. Because the van Hove singularities are smeared out on a scale of few k_BT, this window was too small to reveal individual singularities. Nonetheless, we have shown here that, based on the relative positions of van Hove singularities, significant differences are expected in the rate of charge transfer between SWNTs of different chirality.

To further quantify the extent of these band-structure dependent variations in a way that is directly relevant to experiments, we compare the calculated $k_{ox}-V_{appl}$ curves at small overpotential to Butler−Volmer kinetics, using realistic parameters similar to those of ferrocene(trimethylammonium)$^+$; $V^{0'} = -0.4$ V and $\lambda = 0.5$ eV.[2] The Butler−Volmer formulation is given by $k_{ox} = k^0 \exp((1-\alpha) - e(V_{appl} - V^{0'})/k_BT)$, where k^0 is the standard rate constant and α is the transfer coefficient. In Figure 7a we find that the $k_{ox}-V_{appl}$ curves of the (10,10) and (10,11) SWNTs of Figure 4d can be reasonably fitted by Butler−Volmer for small overpotentials ($|V_{appl} - V^{0'}| < 0.2$ V). We calculated $k_{ox}-V_{appl}$ curves for SWNTs of all possible (n,m), under the condition that the diameter is between 0.4 nm and 5 nm, and fitted the Butler−Volmer equation as was done in Figure 7a. For all SWNTs $V_{hf} = 0.2$ V. The fitting parameters k^0 and α as a function of SWNT diameter are plotted in Figure 7b and c, where every data point represents one SWNT. The variation in the fitted standard rate constant spans about 1 order of magnitude. Furthermore, Figure 7b and c reveal an oscillatory diameter dependence of k^0 and α. This diameter dependence occurs because the energies at which van Hove singularities are situated depend on diameter, and thus singularities shift in and out of the probed region of the DOS as a function of diameter. Because the sequence of van Hove singularities is intrinsically different for metallic and semiconducting SWNTs, one can clearly distinguish different trends between these groups of SWNTs. The discrete jumps in the fitting parameters reflect abrupt, diameter dependent changes in the positions of van Hove singularities.[20] As illustrated in Figure 7b and c, the variations of apparent k^0 and α with diameter for metallic or semiconducting SWNTs are comparable in magnitude to differences between metallic and semiconducting SWNTs at a given diameter.

To further illustrate the consequence of the variation of the apparent standard rate constant for realistic voltammetric experiments taking into account mass transport limitation, we combined the calculated $k_{ox}-V_{appl}$ curves of the SWNTs of Figure 7b and c with the thermodynamic Nernst relation and mass transport limitation using experimental conditions as those given in ref 2.[21] Figure 7d shows the resulting ensemble of voltammograms, as well as the Nernstian limit. Although significant variations occur in the voltammetric curve shape, these variations are not directly related to the metallic or semiconducting nature because the range of apparent k^0 and α values is similar for both types of SWNT. Consequently, when the Fermi level is away from the band gap, we cannot directly distinguish between metallic and semiconducting SWNTs from the curves of Figure 7d.

Charge Transfer when ϵ_F Is Near ϵ_{hf}

Throughout our calculations, we have treated metallic and semiconducting SWNTs using the same formalism. We have however ignored the possibility of potential drops occurring at other impedances in series with the electron transfer impedance. When a semiconducting SWNT is in the "off" state (the Fermi level resides in the band gap), the SWNT becomes highly resistive, and the potential applied to the metal electrode in contact with the SWNT may partially drop at the contacts at the cost of the SWNT−solution interfacial potential difference that drives electron transfer. Whether and to what extent this reduction of interfacial potential difference for SWNTs that are in the "off" state experimentally occurs is likely to be device dependent. Differences in SWNT synthesis, device fabrication, and usage of materials can cause variations in contact resistance, Schottky barrier height, or the presence of gap states due to defects. Day et al.[18] have used SWNT-network devices to indirectly infer that SWNTs in the "off" state accommodate no electrochemical current. On the other hand, we have not observed such behavior experimentally for both individual and

(20) Due to the anisotropy of the energy dispersion near the Fermi points, the energy contours of 2D graphene are not entirely circular. Particularly in metallic SWNTs this can cause a chirality dependent splitting of van Hove singularities near ϵ_{hf}. See ref 6.

(21) To obtain realistic values for the standard rate constant, we set the average value of the standard rate constant in arbitrary units as extracted from Figure 7c to 4 cm/s as was experimentally determined for the oxidation of ferrocene(trimethylammonium)$^+$ at individual SWNT devices in ref 2.

multiple SWNT devices (Heller, I. et al., unpublished experimental results). To concentrate on band structure effects, we have assumed no such series impedance in our calculations.

Conclusions

We have modeled electron transfer kinetics at SWNTs, taking into account the alignment and occupation of solution and electrode states. The occupancy of SWNT states is effectively changed in voltammetry, due to the small SWNT quantum capacitance. Since the rate of electron transfer directly reflects the occupancy and availability of states in both electrolyte and SWNT, one can in principle resolve the density of states of the SWNT in voltammetry with a resolution of the order of k_BT. This interesting effect of electrochemical spectroscopy is a direct consequence of the combination of the small quantum capacitance, distinct electronic structure, and small critical dimension of SWNTs that gives access to electrode kinetics. To experimentally observe the fingerprint of the electronic structure, a redox system with a combination of fast mass transport and slow rate of electron transfer will however need to be used in order to allow accessing kinetics over a wide potential range.

With conventional techniques for SWNT synthesis, the atomic structure cannot be fully controlled, leading to both variations in the electronic structure and the occurrence of a band gap in two-thirds of all SWNTs. Especially important for applications of SWNTs as analytical tools, we have shown that these variations in electronic structure are expected to give rise to intrinsic variations in electron transfer kinetics. When the kinetics are probed over a narrow potential range, diameter dependent oscillations in the rate of electron transfer are expected. Our modeling also shows explicitly that it is a misconception that the electrochemical current is necessarily inhibited when the DOS vanishes at the Fermi level such as in graphene or for semiconducting SWNTs in the "off" state.

The unique combination of properties of SWNTs makes them an excellent model system to gain more insight into the influence of the electronic structure of the electrode on electrochemistry.

Acknowledgment. The authors thank Bernadette Quinn and Hendrik A. Heering for helpful discussions. This work was supported by The Netherlands Organization for Scientific Research (NWO) and the Dutch Foundation for Scientific Research (FOM).

Supporting Information Available: Complete ref 12. This material is available free of charge via the Internet at http://pubs.acs.org.

JA061212K